AFRL-RX-WP-JA-2017-0166

BELOUSOV-ZHABOTINSKY AUTONOMIC HYDROGEL COMPOSITES: REGULATING WAVES VIA ASYMMETRY (POSTPRINT)

Philip R. Buskohl and Richard A. Vaia

AFRL/RX

17 May 2016
Interim Report

(STINFO COPY)

AIR FORCE RESEARCH LABORATORY
MATERIALS AND MANUFACTURING DIRECTORATE
WRIGHT-PATTERSON AIR FORCE BASE, OH 45433-7750
AIR FORCE MATERIEL COMMAND
UNITED STATES AIR FORCE

REPORT DOCUMENTATION PAGE

Form Approved
OMB No. 0704-0188

1. REPORT DATE *(DD-MM-YY)*	2. REPORT TYPE	3. DATES COVERED *(From - To)*
17 May 2016	Interim	30 January 2015 – 17 April 2016

4. TITLE AND SUBTITLE
BELOUSOV-ZHABOTINSKY AUTONOMIC HYDROGEL COMPOSITES: REGULATING WAVES VIA ASYMMETRY (POSTPRINT)

5a. CONTRACT NUMBER
FA8650-11-D-5801-0012

5b. GRANT NUMBER

5c. PROGRAM ELEMENT NUMBER
61102F

6. AUTHOR(S)
Philip R. Buskohl and Richard A. Vaia – AFRL/RX

5d. PROJECT NUMBER
3003

5e. TASK NUMBER 0012

5f. WORK UNIT NUMBER
X0ZH

7. PERFORMING ORGANIZATION NAME(S) AND ADDRESS(ES)
AFRL/RX
Wright-Patterson AFB, OH
45433

8. PERFORMING ORGANIZATION REPORT NUMBER

9. SPONSORING/MONITORING AGENCY NAME(S) AND ADDRESS(ES)
Air Force Research Laboratory
Materials and Manufacturing Directorate
Wright-Patterson Air Force Base, OH 45433-7750
Air Force Materiel Command
United States Air Force

10. SPONSORING/MONITORING AGENCY ACRONYM(S)
AFRL/RXAS

11. SPONSORING/MONITORING AGENCY REPORT NUMBER(S)
AFRL-RX-WP-JA-2017-0166

12. DISTRIBUTION/AVAILABILITY STATEMENT
Distribution Statement A. Approved for public release: distribution unlimited.

13. SUPPLEMENTARY NOTES
PA Case Number: 88ABW-2016-2467; Clearance Date: 17 May 2016. This document contains color. Journal article published in Science Advances, Vol. 190, 23 Sep 2016. © 2016 American Association for the Advancement of Science. The U.S. Government is joint author of the work and has the right to use, modify, reproduce, release, perform, display, or disclose the work.
The final publication is available at doi: 10.1126/sciadv.1600813

14. ABSTRACT *(Maximum 200 words)*
Belousov-Zhabotinsky (BZ) autonomic hydrogel composites contain active nodes of immobilized catalyst (Ru) encased within a nonactive matrix. Designing functional hierarchies of chemical and mechanical communication between these nodes enables applications ranging from encryption, sensors, and mechanochemical actuators to artificial skin. However, robust design rules and verification of computational models are challenged by insufficient understanding of the relative importance of local (molecular) heterogeneities, active node shape, and embedment geometry on transient and steady-state behavior. We demonstrate the predominance of asymmetric embedment and node shape in low-strain, BZ-gelatin composites and correlate behavior with gradients in BZ reactants. Asymmetric embedment of square and rectangular nodes results in directional steady-state waves that initiate at the embedded edge and propagate toward the free edge. In contrast, symmetric embedment does not produce preferential wave propagation because of a lack of diffusion gradient across the catalyzed region.

15. SUBJECT TERMS
Gel composites, synchrony, asymmetry, chemical computing, autonomy

16. SECURITY CLASSIFICATION OF:			17. LIMITATION OF ABSTRACT:	18. NUMBER OF PAGES	19a. NAME OF RESPONSIBLE PERSON (Monitor)
a. REPORT	b. ABSTRACT	c. THIS PAGE			Carlos Suarez
Unclassified	Unclassified	Unclassified	SAR	10	19b. TELEPHONE NUMBER *(Include Area Code)* (937) 255-9184

PHYSICAL SCIENCE

10.1126/sciadv.1600813

Belousov-Zhabotinsky autonomic hydrogel composites: Regulating waves via asymmetry

Philip R. Buskohl and Richard A. Vaia*

Belousov-Zhabotinsky (BZ) autonomic hydrogel composites contain active nodes of immobilized catalyst (Ru) encased within a nonactive matrix. Designing functional hierarchies of chemical and mechanical communication between these nodes enables applications ranging from encryption, sensors, and mechanochemical actuators to artificial skin. However, robust design rules and verification of computational models are challenged by insufficient understanding of the relative importance of local (molecular) heterogeneities, active node shape, and embedment geometry on transient and steady-state behavior. We demonstrate the predominance of asymmetric embedment and node shape in low-strain, BZ-gelatin composites and correlate behavior with gradients in BZ reactants. Asymmetric embedment of square and rectangular nodes results in directional steady-state waves that initiate at the embedded edge and propagate toward the free edge. In contrast, symmetric embedment does not produce preferential wave propagation because of a lack of diffusion gradient across the catalyzed region. The initiation at the embedded edge is correlated with bromide absorption by the inactive matrix, which locally elevates the bromate concentration required for catalyst oxidation. The competition between embedment asymmetry and node geometry was used to demonstrate a repeatable switch in wave direction that functions as a signal delay. Furthermore, signal propagation in or out of the composite was demonstrated via embedment asymmetry and relative dimensions of a T-shaped active network node. Overall, structural asymmetry provides a robust approach to controlling initiation and orientation of chemical-mechanical communication within composite BZ gels.

INTRODUCTION

Mechanically adaptive materials have the intrinsic capacity to swell, morph, or otherwise respond to an external stimulus. Patterning of the mechanical response enables complex motions and shape change, demonstrated in thermally triggered hydrogels (*1*), reprogrammable shape-memory polymers (*2*), responsive liquid crystal elastomers (*3*), and chemically driven Belousov-Zhabotinsky (BZ) gels (*4*–*7*). The coupling of responsive mechanical deformation with local patterning in BZ gels provides fundamental tools for the design of novel devices for remote sensing and energy harvesting and of materials with inherent logic and computing capabilities. However, design criteria for patterning the composite BZ gels, which contain catalyzed and noncatalyzed regions, are needed to program robust chemical-mechanical communication without the need of direct human intervention. This study focuses specifically on the effect of embedment geometry and placement symmetry on the oxidation wave behavior in composite BZ gels, which is key to the flow of chemical information within a BZ device.

The mechanism of chemical-mechanical coupling in BZ monolithic gels has been extensively studied with both experimental and computational approaches [see reviews by Kuksenok *et al.* (*8*) and Yoshida (*9*)]. Briefly, the metal catalyst of the BZ system undergoes a periodic oxidation and reduction that is driven by the local concentration of the initial BZ reagents: nitric acid (HNO_3), malonic acid [$CH_2(COOH)_2$], and sodium bromate ($NaBrO_3$). $HBrO_2$ oxidizes the metal catalyst in a reaction step that simultaneously increases its own supply. The catalyst is then reduced via bromomalonic acid, which generates bromide ions that inhibit the oxidation process. If the metal catalyst is immobilized in a polymer matrix, the oxidation and reduction cycle results in periodic mechanical swelling caused by localized changes in the hydrophobic/hydrophilic behavior of the polymer. For polymers with a lower critical solution temperature (LCST), such as *N*-isopropylacrylamide (NIPAm), this hydrophobic/hydrophilic change shifts the LCST, which may be leveraged to achieve large swelling strains on the order of 20% (*4*, *10*) and up to 500% with microfluidic flow (*11*). Most BZ gel studies are focused on monolith behavior, including maximizing the swelling strain (*12*) and novel actuating geometry (*13*, *14*), or on the relationship between geometry and period behavior (*4*, *7*). Findings from these studies that are relevant for oxidation control include the initiation of waves at corners of shapes (*4*, *7*), synchrony between isolated nodes of active material (*15*, *16*), and characterization of gel constituents with period and swelling behavior (*10*). The BZ reactant and catalyst concentrations used in our gelatin BZ system generate swelling strains in the range of 1 to 2%, which is low in comparison to other BZ systems. However, these BZ conditions produce many (>30) oxidation cycles over the course of the experiment, which enables the investigation of embedment strategies for long-term control of oxidation wave behavior.

Wave propagation, including the initiation site, wave type (target, traveling, and spiral), and direction, is critical for embedded logic and chemical computing. Initial studies on the interaction of chemical waves with diffusion obstacles, such as walls and windows, demonstrated the potential for geometrically regulated excitable and oscillatory media (*17*). For example, the chemical waves of the BZ reaction have been used to determine the optimal path through a maze (*18*) and to create chemical logic gates through oxidation within capillary tubes (*19*, *20*). In these nongel systems, the wave behavior was regulated through the container geometry and/or catalyst patterning. The metal catalyst was localized to the pattern of the maze in the pathfinding study, and the capillary tubes provided diffusion barriers that constrained the waves to create logic gate responses (AND, OR, NOT, etc.). Although it is not the only method used for controlling excitable or oscillatory media (*21*), geometric patterning is an effective approach to preprogramming chemical behavior and is

Functional Materials Division, Materials and Manufacturing Directorate, Air Force Research Laboratory, 2179 12th Street, Wright-Patterson Air Force Base, OH 45433, USA.
*Corresponding author. Email: richard.vaia@us.af.mil

an increasingly attractive approach with the advent of additive manufacturing tools.

BZ gels with an immobilized catalyst are a natural medium to implement geometry-based control strategies because the reaction can be spatially localized. Composite BZ gels, which include regions with and without the metal catalyst, enable the study of hierarchal feedback behaviors due to spatial patterning. For instance, synchrony of oxidation between neighboring active nodes has been computationally predicted (*16*, *22*) and experimentally observed (*5*, *16*, *23*) in composite BZ systems. Chemomechanical syncing in a BZ composite was programmed to generate an amplified cantilever actuator (*5*), and composite node pairs of an active gel were 20 to 30% more likely to oscillate in unison than nonembedded pairs (*23*). In addition, computational models of rectangular-shaped catalyzed gels embedded within a nonactive gel have predicted specific, steady-state wave orientations (*24*). Consistent oxidation wave behavior of this type is an important building block for designing chemical computing and sensing devices with composite BZ gels.

Here, we experimentally investigate the role of asymmetry to regulate the steady-state oxidation behavior of composite BZ gels. Square and rectangle geometries of the active gel are embedded in symmetric and asymmetric configurations of the nonactive gel, enabling the comparison of active gel placement and embedment symmetry. Oxidation waves have predictable steady-state behavior when the embedment boundary condition creates a diffusion gradient. We demonstrate the utility of this concept for the design of a signal delay and the control of wave splitting in a T-junction. Collectively, this work adds to the understanding of composite gel synchrony, experimentally confirms previous computational predictions of BZ gel behavior, and extends the programming tools of oriented oxidation behavior for BZ device design.

RESULTS

Composite embedment conditions

Composite BZ gels consist of active and nonactive regions. Although only the active regions undergo autonomous oscillations, the nonactive material maintains the spacing between active regions and controls which surfaces of the active gel have direct exposure to the BZ solution. To evaluate the effect of embedment on the wave direction of Ru oxidation, we placed square nodes of active material in several embedment configurations (Fig. 1). The symmetry of embedment is classified according to whether the reflection symmetry of the horizontal (*H-H*) and vertical (*V-V*) axes is maintained (Fig. 1A). For example, a gel with the top and bottom embedded, but not the left and right, is symmetric because, independently, each axis sees the same embedment condition about itself. In contrast, in the asymmetric cases in Fig. 1B, one or more of the reflection symmetries about the vertical and horizontal axis are broken. In all of the symmetric configurations, there was no preferential direction of the oxidation wave. However, when asymmetrically embedded, the oxidation wave consistently traveled from the gel interior toward the exterior BZ solution. Steady-state waves traveled along the diagonal of the corner embedded node (137° ± 21°) and perpendicular to the center edge of the three-sided embedded node (188° ± 21°). Target waves are intermittently observed in symmetrically embedded gels, similar to previous reports in nonembedded gels (*4*).

Diffusion gradient and bromide initiation mechanism

We deduce that asymmetric embedment creates a diffusion gradient of BZ reactants that preferentially orients oxidation waves along the axis of the gradient. The gradient aligns with the diagonal of the active square node when two adjacent sides are embedded and is parallel to the horizontal axis when three sides are embedded (Fig. 1B). The presence of a reactant gradient is an intuitive conclusion because BZ reactants and by-products face less resistance to mass transport at edges exposed to the BZ solution compared to edges embedded in the polymer network. However, which end of the diffusion gradient should the oxidation wave initiate? To address this question, we recall the Field-Koros-Noyes reaction mechanism (*25*), which summarizes the kinetics of the BZ reaction with three basic processes

$$(1)\ BrO_3^- + 2Br^- + 3H^+ \rightarrow 3HOBr$$

$$(2)\ HBrO_2 + BrO_3^- + 3H^+ + 2M_{red} \rightarrow 2HBrO_2 + 2M_{ox} + H_2O$$

$$(3)\ 2M_{ox} + BrMA + MA \rightarrow 2M_{red} + fBr^- + \text{other products}$$

In step 1, bromate (BrO_3^-) and bromide (Br^-) react to create hypobromous acid. As discussed in the Introduction, bromous acid and bromate facilitate the conversion of the metal catalyst from the reduced (M_{red}) to the oxidized (M_{ox}) state in step 2. In step 3, bromomalonic acid reduces the metal catalyst, producing bromide and other products. If the embedding matrix acts as a diffusive barrier equally to all BZ reactants, we would anticipate an increased accumulation of bromide ions at the embedded edges of the active gel compared with the nonembedded edges exposed to the BZ solution. Elevated bromide concentrations would reduce the local bromate concentration via step 1 and consequently inhibit the oxidation of the metal catalyst on the embedded side of the diffusion gradient. On the other hand, if there is preferential depletion of bromide by the surrounding inactive matrix, the concentration of bromate available to oxidize the metal catalyst would increase, biasing oxidation at the embedded side. The composite gelatin specimens (Fig. 1) initiate at the embedded corner, suggesting that, rather than creating a uniform diffusion barrier, the plain embedding gelatin preferentially sequesters molecular species.

To test this hypothesis, we placed square nodes of active gelatin in notched corners of a glass slide to simulate a diffusion barrier and polydimethylsiloxane (PDMS) to simulate preferential bromide depletion by the surrounding inactive matrix (Fig. 2). For glass, the oxidation waves consistently initiated at the corner of the active node exposed to the BZ solution and propagated along the diagonal of the node to the embedded corner (Fig. 2A). The orientation angle was 320° ± 18° (mean ± SD) averaged across 15 specimens. Line cuts along the diagonal (a-a′) demonstrate that the oxidation waves travel toward the gel interior with time (see movie S1). This is consistent with the glass acting as a diffusion barrier that inhibits the initiation of oxidation at the embedded interface. In contrast, a PDMS corner notch (Fig. 2B) generated wave orientations traveling away from the notch (Fig. 2B and movie S2). PDMS is a known bromide absorber, as observed in previous BZ solution–based studies (*26*, *27*), and simulates a diffusion gradient with a selectively reduced bromide environment at the embedded interface. The slope of the oxidation wave in the parallel line cut (a-a′) is nearly identical to the rigidly embedded corner node in gelatin (PDMS: 142° ± 17° versus gelatin-embedded: 137° ± 21°). We suspect that a similar mechanism may be at play in the gelatin-embedded specimens because bromide

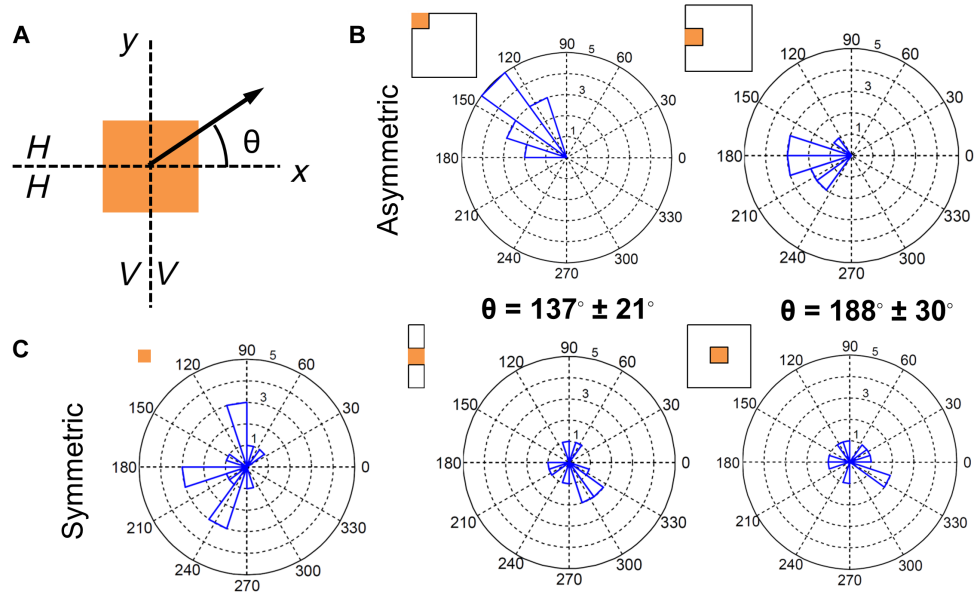

Fig. 1. Oxidation wave direction is dependent on embedment symmetry. (**A**) Schematic of reflection symmetry about the horizontal (*H-H*) and vertical (*V-V*) axes and the definition of the orientation angle, θ. (**B**) Asymmetric embedment conditions with one or more broken reflection symmetries generate oriented waves. (**C**) Symmetric embedment conditions with reflection symmetries intact show no preferential wave orientation. Mean orientation angle was averaged over a minimum of 50 oscillations after $t > 100$ min. Data are means ± SD across $n \geq 10$ specimens.

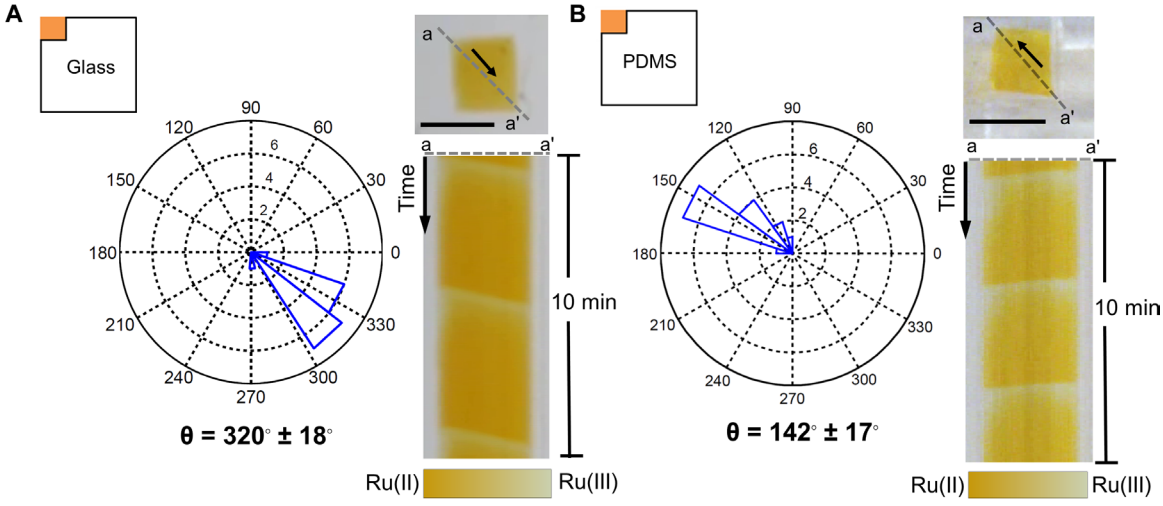

Fig. 2. Oxidation wave direction is diffusion-dependent. (**A**) Diffusion barrier case study. Oxidation waves initiate in the corner node exposed to the BZ solution and propagate toward the embedded corner when placed in contact with the glass boundary. Scale bar, 1 mm. (**B**) Bromide sequester case study. BZ gels placed in contact with the PDMS boundary initiate oxidation waves at the embedded corner and propagate toward the corner node exposed to the BZ solution. Data are means ± SD across 15 specimens. Line cuts parallel (a-a') to wave direction over 10 min demonstrate the difference in wave direction. Scale bar, 1 mm.

uptake by gelatin has been observed in the photographic gel research community (*28*). Together, these results indicate that local bromide concentrations and a diffusion gradient, induced through embedment, are capable of regulating the steady-state orientation and local initiation of BZ oxidation waves.

Non-unity aspect ratio BZ gels

BZ oxidation waves travel along the long dimension of non-unity aspect ratio (AR) gels, as previously predicted by simulation (*24*) and demonstrated experimentally in nonembedded gels (*4*). Similar behavior is observed in nongel BZ systems, where the catalyst is patterned on a substrate, such as a Cartesian maze (*18*) or channels ahead of a logic gate (*20*). The apparent proclivity to oxidize along the long axis is, in part, a consequence of the short characteristic diffusion length of the BZ solution (30 μm) (*23*), which quickly oxidizes across the short axis of the rectangle (approximately 0.5 mm). It is expected that multiple oxidation waves, without preferential orientation, would simultaneously occur if the rectangular film was larger or if a BZ solution concentration with a shorter

characteristic diffusion length was used. We speculate that the oxidation waves could orient parallel to the short axis of a catalyzed strip in our current system if (i) the embedded pattern was a set of small, concentric rings with a target wave initiated at the center or (ii) the rectangular specimen was oriented perpendicular to a flow field of the BZ solution, which would dominate the natural diffusion process of the system. When not embedded, the steady-state oxidation waves initiate from the center of the gel and travel along the long dimension toward the gel edges (Fig. 3A and movie S3). However, when fully embedded, the steady-state waves initiate from the short edges of the gel and travel toward the center (Fig. 3B and movie S4). Edge initiation in embedded gels was previously predicted with a computational model of a NIPAm BZ gel (*24*) but had not been experimentally verified.

Non-unity AR gels can also be embedded asymmetrically, with either a short edge or a long edge exposed. In both cases, the oxidation waves were oriented along the long dimension of the gel (Fig. 4). BZ gels embedded with only one long edge exposed to the BZ solution showed no directional bias (AR = 3.4 ± 0.4, n = 5). Oxidation waves would initiate from either end of the long axis and continue to initiate from that edge for the remainder of the experiment. The direction is likely dependent on secondary effects, such as the local initial BZ reactant concentrations and geometric imperfections in the gel. An example of both left (three of five specimens) and right (two of five specimens) oxidation waves over a 5-min time window is shown in Fig. 4A (see also movie S5). In contrast, steady-state waves in BZ composites with the long axis embedded perpendicular to the embedding matrix edge consistently traveled from the gel interior to the exterior BZ solution (AR = 2.9 ± 0.4, n = 5). A representative line plot of this steady-state behavior over 10 min is shown in Fig. 4B, and a video of this embedment condition is included in the Supplementary Materials (movie S6). The preferential steady-state wave direction of this embedment condition, which highlighted the potential of embedment boundary conditions for wave control, was computationally predicted by Yashin *et al.* (*24*). The asymmetry of diffusion behavior between embedded and free edge contributes to this preferential wave direction.

In non-unity AR gels that are embedded perpendicular to the matrix edge (bulk-embedded), a consistent switch in oxidation wave direction is observed. Before reaching steady state, oxidation waves initially travel toward the gel interior, but the wave propagation eventually switches toward the free edge of the gel. Figure 5A shows the representative wave switch of a single specimen as a plot of the location of initial oxidation for each wave versus the run time of the experiment (see movie S7). The initial oxidation location is approximated by the first signal peak detected for each wave along the a-a′ line cut. The switch between edge and interior point initiations was curve-fit with a hyperbolic tangent function, defined as $x = L/2 \tanh[k(t - t_s)] + L/2$, where L is the length of the Ru-immobilized strip, t_s is the transition time, and k is the transition rate. The average transition time across specimens was t_s = 108 ± 26 min, and the transition rate was $k = 0.06 \pm 0.03$ min^{-1} (mean ± SD; n = 6). The initiation point migrates toward the embedded end of the Ru gel in a noisy, but measurable, manner (Fig. 5). One possible mechanism for the wave switch is the differential shrinkage between the catalyzed and plain embedding gel when initially placed in the BZ solution due to the mismatch in ionic strengths. However, gel shrinkage plateaus after 25 min (see fig. S1), which does not correlate with the wave transition time that occurs closer to the 100-min mark. Instead, the transition is more likely a consequence of the embedded edge reaching a sufficiently decreased bromide concentration relative to the rest of the active gel to preferentially initiate oxidation waves at the embedded edge. This aligns with the diffusion gradient and bromide mechanism identified in the asymmetric square node results.

The wave switching observed in the bulk-embedded gel could have applications in BZ systems with a preferential delay in steady-state behavior, perhaps for synchronizing with other catalyzed regions or for timing with an external event. Although this study focuses on the effect of embedment conditions on steady-state behavior, time-dependent effects, such as the wave switch, initial gel shrinkage, and reaction transients, are important for further study.

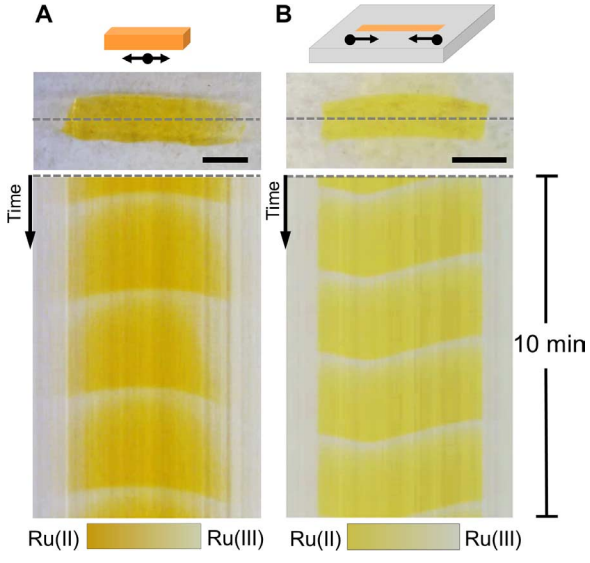

Fig. 3. Oxidation wave direction in non-unity AR gels is dependent on embedment. (**A** and **B**) Schematic indicating wave direction in a (A) non-embedded and (B) embedded rectangular gel. Line plot of signal intensity along the gel centerline versus time for a nonembedded and embedded gel. Scale bars, 1 mm.

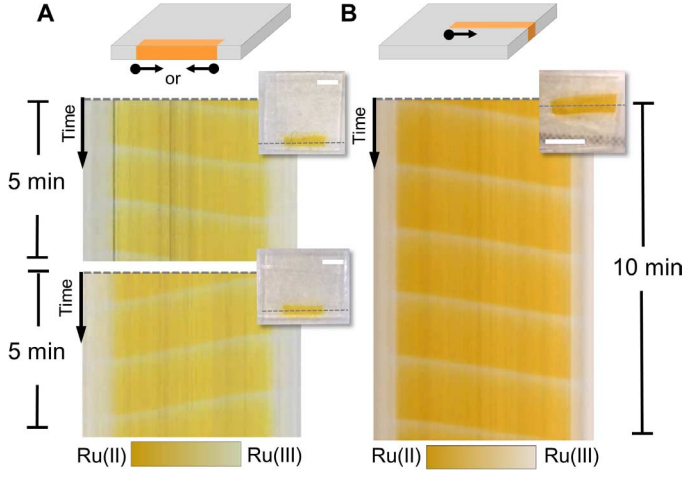

Fig. 4. Surface and bulk-embedded specimens have preferential wave orientations. (**A**) Waves remain along the long dimension of the gel even when asymmetrically embedded. Left or right directionality is dependent on secondary effects, such as geometric irregularities and local BZ reactant concentrations. (**B**) Waves travel toward the gel edge if the direction aligns with the long dimension of the gel. Scale bars, 1 mm.

Node geometry versus embedment condition

Steady-state waves of surface-embedded specimens prefer to travel along the active strip from either edge, rather than initiate at the center (Fig. 4A), whereas bulk-embedded steady-state waves preferentially orient toward the exterior of the embedding gel (Fig. 4B). These steady-state behaviors of bulk and surface-embedment configurations were placed in direct competition with each other using a "T"-shaped geometry. For instance, if the surface-embedded behavior is dominant, oxidation waves will travel toward the gel interior. However, if the bulk-embedded behavior is dominant, waves traveling toward the exterior will drive an atypical center initiation for the surface-embedded strip. The test was performed for a set of bulk-embedded (l_b) and surface-embedded (l_s) lengths to determine the dominant steady-state behavior. Figure 6 shows the return map profiles of steady-state oscillations for 60 min (t = 420 to 480 min). The return map correlates the catalyst oxidation state between the three ends of the T, denoted by the black nodes labeled I, II, and III in the schematics of Fig. 6. L-shaped return maps indicate node pairs whose oxidation [Ru(III) state] is antiphase, whereas return maps populated along the diagonal of the plot indicate in-phase oxidation. The bulk-embedded steady-state behavior was dominant for l_s/l_b = 0.6 and 1.3, with waves initiating from the gel interior and splitting when they reached the vertex of the T. Figure 6 (A and B) depicts this result through (i) the in-phase oxidation of nodes I and II, which share the split signal, and (ii) the antiphase oxidation of nodes I and III due to node III driving the signal toward node I. At the higher ratio l_s/l_b = 2.1, the surface-embedded steady-state behavior was dominant, sending waves along the active strip and into the bulk interior. Figure 6C indicates this trend through the L-shaped return

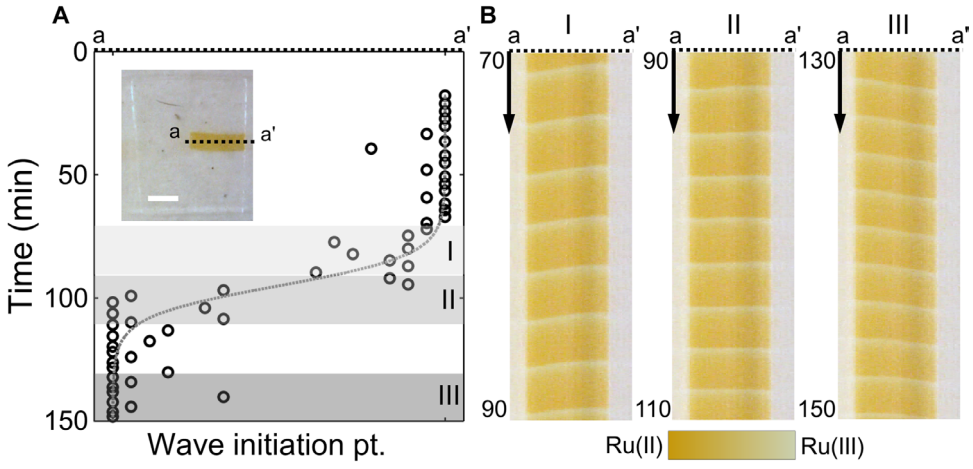

Fig. 5. Wave direction switches in bulk-embedded specimens. (**A**) Representative plot of wave initiation point along the catalyzed gel as a function of time. Initiation of the BZ wave transitions from solution edge to embedded edge at approximately 100 min. Inset: Image of bulk-embedded gel and line cut a-a'. (**B**) Line plots of BZ gel (I) before, (II) during, and (III) after the transition. Scale bar, 1 mm. A movie file of the wave switch behavior is included in the Supplementary Materials (movie S7).

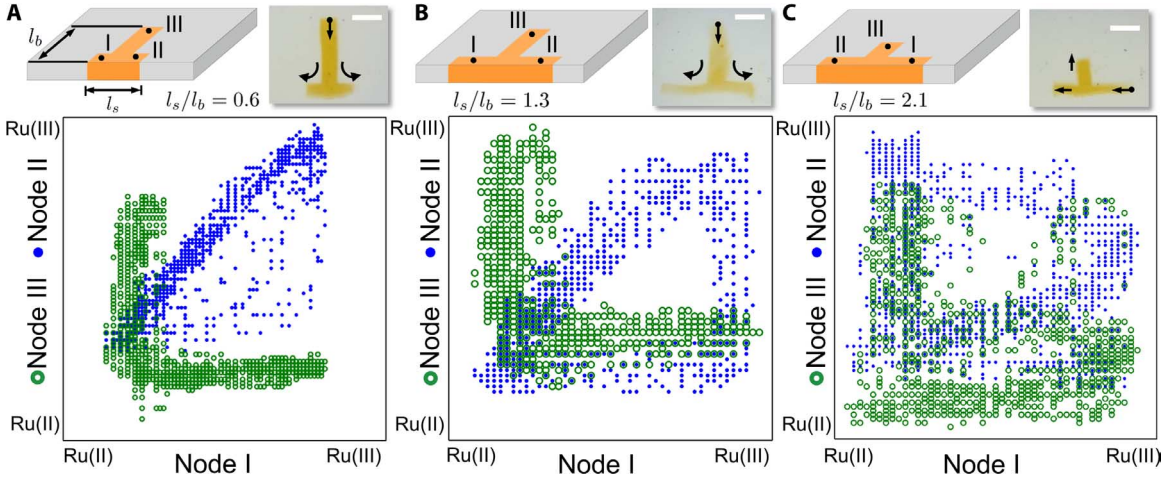

Fig. 6. T-specimen geometry indicates preference of interior node wave initiation. (**A** to **C**) Schematic of T-specimen geometry, top view image of the sample, and return map of Ru oxidation cycle shown for specimens with (A) l_s/l_b = 0.6, (B) l_s/l_b = 1.3, and (C) l_s/l_b = 2.1. The return map correlates the catalyst oxidation state between the three nodes (I, II, and III) denoted in the schematic. Nodes I and II transition from in-phase oxidation to antiphase with increasing l_s/l_b (blue dots). Nodes I and III are consistently out of phase because node III drives node I for l_s/l_b = 0.6 and 1.3 or node I drives node III for l_s/l_b = 2.1. Scale bars, 1 mm. Movie files of these gels are included in the Supplementary Materials (movies S8, S9, and S10).

maps for nodes II and III, which are both driven by the wave initiation at node I. The breakdown of the bulk-dominant behavior in Fig. 6C is likely due to the reduced length of the bulk-embedded strip, which reduces the diffusion gradient of BZ intermediate reactants and decreases the time for an interior oxidation event to reset before an oxidation occurs on the surface. Collectively, the results of the T-specimen study suggest that the diffusion mechanism observed in the asymmetrically embedded square nodes and the bulk-embedded strip scenario is sufficient to deterministically program steady-state wave directions through a bulk and surface-embedded junction. Additional studies are needed to confirm the reliability of steady-state waves over a larger range of l_s/l_b ratios and in networks with multiple junctions, but these results provide initial guidance for the BZ device design.

DISCUSSION

The composite BZ gels investigated in this study demonstrated that steady-state oxidation wave behavior can be controlled by the asymmetry of the embedment boundary conditions. In each case, preferential wave direction required asymmetry of embedment condition (Fig. 1) or nonunity AR geometry, such as the rectangular strip, which biased the wave to travel along the long axis (Figs. 3 and 4). Therefore, geometry and symmetry present two tools for the BZ composite gel designer: (i) control active regions with asymmetric embedment and (ii) use active region geometry to constrain the domain of oxidation waves. Controlling the direction of oxidation through patterning of active regions has previously been used in nonembedded BZ gels. For instance, a linear array of oriented triangular BZ gels showed a preferential wave direction (*15*), and asymmetries in catalyst concentration and active node size were also shown to bias the oxidation wave direction (*16*). However, the added control enabled by composite gel boundary conditions significantly extends the programmability of BZ devices. For instance, embedment of rectangular active strips relocated the wave initiation site from the center of nonembedded active gels to the edges (Fig. 3), highlighting how boundary conditions regulate the BZ process.

Asymmetry in this context of composite gel boundary conditions is focused on repeatable, predetermined control of steady-state behavior. This is in contrast to symmetry breaking in BZ gels where heterogeneities in reactant concentration or specimen geometry induce a bifurcation in chemomechanical behavior. For example, slight gradients in cross-linking, reactant concentration, or specimen geometry determine whether clockwise or counterclockwise rotation occurs in symmetrically compressed BZ gels (*29*) and are responsible for the occurrence of traveling waves in specimens that are computationally predicted to produce target waves (*7*). Heterogeneities of this nature are also responsible for the variability in wave direction observed in the symmetrically embedded square specimens in Fig. 1. The programming of asymmetric diffusion gradients through composite embedment overcomes these natural experimental heterogeneities of the BZ system to generate consistent steady-state wave behavior. External stimuli, such as light (*30*) or heat (*31*), have also been used to trigger symmetry breaking in BZ systems. In contrast, embedment passively guides oxidation behavior without further input of energy or other intervention during the BZ reaction, which better leverages the autonomous nature of the BZ system.

The preferential location of wave initiation along the diffusion gradient correlates with local bromide concentrations, as shown in the glass and PDMS test cases in Fig. 2. The bromide mechanism has been previously observed in a BZ solution–based study with PDMS boundaries but has been underutilized in BZ gels studies, which predominantly use chemically inert polymers, such as NIPAm (*4*, *6*). The bromide mechanism enables additional design possibilities in multimaterial systems where oxidation waves could orient away or toward an embedded edge depending on the embedding material. The role of diffusion is likely heightened in our low–swelling gelatin system (1 to 2%) compared to higher–swelling NIPAm systems (>20%) (*4*, *10*), where mechanical confinement from embedment could play a larger role. Computational models of composite BZ gel systems have predicted that the chemomechanical swelling reinforces the coupling between neighboring regions of the active gel, increasing the likelihood of in-phase synchrony via the mechanical deformation of the embedding matrix (*22*, *32*). The large swelling BZ systems could possibly trigger oxidation waves in adjacent active regions via mechanical communication, overriding the intended diffusion barrier of the embedding boundary conditions. In this case, local stiffening of the embedding gel may be required to ensure that mechanical and chemical signals operate as intended. Local control of gel stiffness could be achieved through photoinitiated polymerization (*7*, *33*). Stiffness patterning in a high-strain BZ system could lead to unique device-level hierarchal control, where chemical and/or mechanical communication specifically regulates the direction of catalyst oxidation.

The delayed wave switch of bulk-embedded strips and the preference for exterior-directed oxidation in T-shaped specimens are two additional design concepts for BZ devices. Arrays of bulk-embedded gel could possibly be programmed to switch direction with phase delay using different embedded lengths. This could be relevant for timing an external event that could be triggered through a visual readout of the wave patterns. Furthermore, T-shaped nodes are prime candidates for initiating chemical communication within a BZ circuit, but additional research is needed to identify interaction effects that will occur in larger patterns of active gel.

In summary, embedment asymmetry creates a diffusion gradient that can be leveraged for chemomechanical control of oxidation behavior in composite BZ gels. Active node shape and embedment provide a means to overcome local heterogeneities and control macroscopic behavior. Mechanical confinement may play an important role in BZ systems with higher swelling strains, which would enable an additional approach to regulating the oxidation wave behavior and would merit further study. Signal propagation in or out of the composite gel was demonstrated via embedment asymmetry and relative dimensions of a T-shaped active network node, highlighting how patterning in a composite system can generate device-like functionality. Overall, structural asymmetry provides a robust approach to controlling initiation and orientation of chemical-mechanical communication within composite BZ gels and will continue to be an important consideration in moving to larger, device-level, BZ gel networks.

MATERIALS AND METHODS

Synthesis of the Ru gelatin

All specimens consisted of 10% type A gelatin (~300 bloom) acquired from Sigma. Plain gelatin was fabricated from deionized water in a 2 g:20 ml ratio. The Ru catalyst was immobilized within the gel using a succinimidyl ester strategy that targets the amine group on the amino acid lysine of the gelatin network, as previously described (*5*, *23*). "Active" gelatin was fabricated at the same ratio with sodium phosphate buffer

(SPB; pH 7.4), which enhanced Ru incorporation by reducing the premature hydrolysis of the activated ester. Bis(2,2′-bipyridine)-4′-methyl-4-carboxybipyridine-ruthenium *N*-succinimidyl ester-bis (hexafluorophosphate) (Sigma 96631) was added in a ratio of 4.1 mg:250 mg 10% SPB gelatin in increments while heated at 42° to 46°C for 2 to 4 hours. Small amounts of *N*,*N*-dimethylformamide (~10 to 40 μl) may be added to assist in the dissolution of the catalyst.

Composite specimen fabrication

Using the thermogel properties of gelatin, we first poured liquid gelatin into molds to create thin films (0.4 to 1 mm thick) that congealed at room temperature (22° to 24°C). Segments of these films were then manually cut, placed in a pattern, and backfilled with liquid plain gelatin (~46°C). The elevated temperature of the plain gelatin not only facilitates pouring during backfill but also promotes mechanical connection to the active gelatin through the entanglement of the polymer chains. For square nodes, a single strip of active gelatin was embedded in a rectangular prism of plain gelatin that was then sliced using a custom cutting jig (see fig. S2). For the non-unity AR gels, a rectangular film of active gelatin was embedded and cut. Average section thickness was 0.5 mm.

Ru concentration measurement

Ultraviolet-visible spectroscopy was used to quantify the Ru concentration in fully hydrated specimens, as previously described (*23*). Hydrated sections of gel (~0.5 mm thick) were placed between quartz slides with a known separation distance. The molar absorptivity coefficient for $Ru(bpy)_3^{2+}$ is $\varepsilon = 14{,}600\ M^{-1}\ cm^{-1}$ at $\lambda = 452$ nm (*34*, *35*). Applying the Beer-Lambert law and correcting for polymer absorbance, the average Ru concentration across batches was 0.6 ± 0.3 mM in swollen gels.

Quantification of BZ wave behavior

Composite BZ gels were placed in 5 ml of unstirred BZ reactants at room temperature (22° to 24°C), and a video was recorded with a Dino Cam for 5 hours. The initial concentrations of the BZ reagents were 0.7 M nitric acid (HNO_3), 0.08 M sodium bromate ($NaBrO_3$), and 0.04 M malonic acid [$CH_2(COOH)_2$]. These initial concentrations were selected to achieve short oxidation periods (<3 min) and generate >100 oscillations over the course of the experiment. Previously reported empirical relationships between period and the initial reactant concentrations for gelatin guided the selection (*36*). To quantify the oxidation behavior, the signal intensity of the blue channel was extracted from the video at specific locations in the Ru-immobilized sections of the composite gel. The oxidation period was calculated as the difference in time between the oxidation peaks of the signal intensity curve. For square nodes, a 3 × 3 grid of signal intensity was sampled as shown in fig. S3A. The peaks of the signal intensity versus time curves, which correspond to the oxidation of Ru, were determined for each node using the "findpeaks.m" algorithm within MATLAB (hollow circles in fig. S3B). The oxidation wave orientation, θ_i, for $i = 1$ to 9 was calculated by comparing the time of oxidation between the nodes of the grid with the center node (#5). The orientation angle was defined with respect to the positive x axis and was averaged across all nine nodes for each oxidation oscillation. The steady-state orientation angle for each specimen was calculated as the average θ between 100 and 300 min in the BZ solution (fig. S3D). The summary orientation angle for each embedment condition was presented as an average of the steady-state angles across specimens ($n \geq 10$). For rectangular gels, the oscillation behavior was sampled along the long axis of the active gel and was presented using representative line plots. The oxidation wave intensities of T-shaped specimens were evaluated at select nodes, as denoted in the text and figure schematics.

SUPPLEMENTARY MATERIALS

Supplementary material for this article is available at http://advances.sciencemag.org/cgi/content/full/2/9/e1600813/DC1

fig. S1. Initial gel shrinkage is not correlated with wave reversal.
fig. S2. Custom cutting jig for sectioning of composite hydrogels.
fig. S3. Quantification of orientation angle.
movie S1. Glass notch study (speed, 4×; scale bar, 1 mm).
movie S2. PDMS notch study (speed, 4×; scale bar, 1 mm).
movie S3. Nonembedded rectangular strip (speed, 4×; scale bar, 1 mm).
movie S4. Fully embedded rectangular strip (speed 4×; scale bar, 1 mm).
movie S5. Surface-embedded rectangular strip (speed, 4×; scale bar, 1 mm).
movie S6. Bulk-embedded rectangular strip (speed, 4×; scale bar, 1 mm).
movie S7. Bulk-embedded wave switch (speed, 8×; scale bar, 1 mm).
movie S8. T-shaped specimen ($l_s/l_b = 0.6$; speed, 4×; scale bar, 1 mm).
movie S9. T-shaped specimen ($l_s/l_b = 1.3$; speed, 4×; scale bar, 1 mm).
movie S10. T-shaped specimen ($l_s/l_b = 2.1$; speed, 4×; scale bar, 1 mm).

REFERENCES AND NOTES

1. J. Kim, J. A. Hanna, M. Byun, C. D. Santangelo, R. C. Hayward, Designing responsive buckled surfaces by halftone gel lithography. *Science* **335**, 1201–1205 (2012).
2. R. R. Kohlmeyer, P. R. Buskohl, J. R. Deneault, M. F. Durstock, R. A. Vaia, J. Chen, Shape-reprogrammable polymers: Encoding, erasing, and re-encoding. *Adv. Mater.* **26**, 8114–8119 (2014).
3. T. H. Ware, M. E. McConney, J. J. Wie, V. P. Tondiglia, T. J. White, Voxelated liquid crystal elastomers. *Science* **347**, 982–984 (2015).
4. I. C. Chen, O. Kuksenok, V. V. Yashin, R. M. Moslin, A. C. Balazs, K. J. Van Vliet, Shape- and size-dependent patterns in self-oscillating polymer gels. *Soft Matter* **7**, 3141–3146 (2011).
5. M. L. Smith, C. Slone, K. Heitfeld, R. A. Vaia, Designed autonomic motion in heterogeneous Belousov–Zhabotinsky (BZ)-gelatin composites by synchronicity. *Adv. Funct. Mater.* **23**, 2835–2842 (2013).
6. R. Yoshida, T. Takahashi, T. Yamaguchi, H. Ichijo, Self-oscillating gel. *J. Am. Chem. Soc.* **118**, 5134–5135 (1996).
7. P. Yuan, O. Kuksenok, D. E. Gross, A. C. Balazs, J. S. Moore, R. G. Nuzzo, UV patternable thin film chemistry for shape and functionally versatile self-oscillating gels. *Soft Matter* **9**, 1231–1243 (2013).
8. O. Kuksenok, D. Deb, P. Dayal, A. C. Balazs, Modeling chemoresponsive polymer gels. *Annu. Rev. Chem. Biomol. Eng.* **5**, 35–54 (2014).
9. R. Yoshida, Self-oscillating gels driven by the Belousov–Zhabotinsky reaction as novel smart materials. *Adv. Mater.* **22**, 3463–3483 (2010).
10. R. C. Kramb, P. R. Buskohl, M. J. Dalton, R. A. Vaia, Belousov–Zhabotinsky hydrogels: Relationship between hydrogel structure and mechanical response. *Chem. Mater.* **27**, 5782–5790 (2015).
11. Y. Zhang, N. Zhou, N. Li, M. Sun, D. Kim, S. Fraden, I. R. Epstein, B. Xu, Giant volume change of active gels under continuous flow. *J. Am. Chem. Soc.* **136**, 7341–7347 (2014).
12. R. Yoshida, M. Tanaka, S. Onodera, T. Yamaguchi, E. Kokufuta, In-phase synchronization of chemical and mechanical oscillations in self-oscillating gels. *J. Phys. Chem. A* **104**, 7549–7555 (2000).
13. S. Maeda, Y. Hara, T. Sakai, R. Yoshida, S. Hashimoto, Self-walking gel. *Adv. Mater.* **19**, 3480–3484 (2007).
14. S. Maeda, Y. Hara, R. Yoshida, S. Hashimoto, Peristaltic motion of polymer gels. *Angew. Chem.* **120**, 6792–6795 (2008).
15. S. Tateyama, Y. Shibuta, R. Yoshida, Direction control of chemical wave propagation in self-oscillating gel array. *J. Phys. Chem. B* **112**, 1777–1782 (2008).
16. V. V. Yashin, S. Suzuki, R. Yoshida, A. C. Balazs, Controlling the dynamic behavior of heterogeneous self-oscillating gels. *J. Mater. Chem.* **22**, 13625–13636 (2012).
17. J. A. Sepulchre, A. Babloyantz, Propagation of target waves in the presence of obstacles. *Phys. Rev. Lett.* **66**, 1314–1317 (1991).
18. O. Steinbock, Á. Tóth, K. Showalter, Navigating complex labyrinths: Optimal paths from chemical waves. *Science* **267**, 868–871 (1995).
19. O. Steinbock, P. Kettunen, K. Showalter, Chemical wave logic gates. *J. Phys. Chem.* **100**, 18970–18975 (1996).
20. A. Toth, V. Gaspar, K. Showalter, Signal transmission in chemical systems: Propagation of chemical waves through capillary tubes. *J. Phys. Chem.* **98**, 522–531 (1994).

21. A. S. Mikhailov, K. Showalter, Control of waves, patterns and turbulence in chemical systems. *Phys. Rep.* **425**, 79–194 (2006).
22. V. V. Yashin, A. C. Balazs, Chemomechanical synchronization in heterogeneous self-oscillating gels. *Phys. Rev. E* **77**, 046210 (2008).
23. P. R. Buskohl, R. C. Kramb, R. A. Vaia, Synchronicity in composite hydrogels: Belousov–Zhabotinsky (BZ) active nodes in gelatin. *J. Phys. Chem. B* **119**, 3595–3602 (2015).
24. V. V. Yashin, O. Kuksenok, A. C. Balazs, Modeling autonomously oscillating chemo-responsive gels. *Prog. Polym. Sci.* **35**, 155–173 (2010).
25. R. J. Field, E. Koros, R. M. Noyes, Oscillations in chemical systems. II. Thorough analysis of temporal oscillation in the bromate-cerium-malonic acid system. *J. Am. Chem. Soc.* **94**, 8649–8664 (1972).
26. B. T. Ginn, B. Steinbock, M. Kahveci, O. Steinbock, Microfluidic systems for the Belousov–Zhabotinsky reaction. *J. Phys. Chem. A* **108**, 1325–1332 (2004).
27. O. Steinbock, S. C. Müller, Radius-dependent inhibition and activation of chemical oscillations in small droplets. *J. Phys. Chem. A* **102**, 6485–6490 (1998).
28. W. Cooper, The bromination of gelatin. *Photogr. Sci. Eng.* **4**, 160–166 (1960).
29. O. Kuksenok, V. V. Yashin, A. C. Balazs, Mechanically induced chemical oscillations and motion in responsive gels. *Soft Matter* **3**, 1138–1144 (2007).
30. P. Dayal, O. Kuksenok, A. C. Balazs, Reconfigurable assemblies of active, autochemotactic gels. *Proc. Natl. Acad. Sci. U.S.A.* **110**, 431–436 (2013).
31. R. C. Kramb, P. R. Buskohl, C. Slone, M. L. Smith, R. A. Vaia, Autonomic composite hydrogels by reactive printing: Materials and oscillatory response. *Soft Matter* **10**, 1329–1336 (2014).
32. V. V. Yashin, K. J. Van Vliet, A. C. Balazs, Controlling chemical oscillations in heterogeneous Belousov-Zhabotinsky gels via mechanical strain. *Phys. Rev. E* **79**, 046214 (2009).
33. Y. Zhang, R. Zhou, J. Shi, N. Zhou, I. R. Epstein, B. Xu, Post-self-assembly cross-linking to integrate molecular nanofibers with copolymers in oscillatory hydrogels. *J. Phys. Chem. B* **117**, 6566–6573 (2013).
34. K. Kalyanasundaram, Photophysics, photochemistry and solar energy conversion with tris(bipyridyl)ruthenium(II) and its analogues. *Coord. Chem. Rev.* **46**, 159–244 (1982).
35. C. T. Lin, W. Böttcher, M. Chou, C. Creutz, N. Sutin, Mechanism of the quenching of the emission of substituted polypyridineruthenium(II) complexes by iron(III), chromium(III), and europium(III) ions. *J. Am. Chem. Soc.* **98**, 6536–6544 (1976).
36. M. L. Smith, K. Heitfeld, M. Tchoul, R. A. Vaia, paper presented at the SPIE Smart Structures and Materials+ Nondestructive Evaluation and Health Monitoring, San Diego, CA, 23 March 2011.

Acknowledgments: We thank A. Balazs, V. Yashin, and O. Kuksenok for their helpful discussions regarding this study and the reviewer who assisted with the identification of the bromide initiation mechanism. We also thank A. Safriet for the design and fabrication of the gelatin cutting jig. **Funding:** We acknowledge the support from the Air Force Office of Scientific Research (grant #13RX08COR) and the Air Force Research Laboratory's Materials and Manufacturing Directorate. **Author contributions:** P.R.B. designed, performed, and analyzed all the experiments in this study and drafted the manuscript. R.A.V. provided technical guidance, secured required funding, and reviewed the manuscript. **Competing interests:** The authors declare that they have no competing interests. **Data and materials availability:** All data needed to evaluate the conclusions in the paper are present in the paper and/or the Supplementary Materials. Additional data related to this paper may be requested from the authors.

Submitted 17 April 2016
Accepted 16 August 2016
Published 23 September 2016
10.1126/sciadv.1600813

Citation: P. R. Buskohl, R. A. Vaia, Belousov-Zhabotinsky autonomic hydrogel composites: Regulating waves via asymmetry. *Sci. Adv.* **2**, e1600813 (2016).